Tenth International Conference on Computational Fluid Dynamics (ICCFD10), Barcelona,Spain, July 9-13, 2018

ICCFD10-2018-377

Stability properties of a Fluid-Structure Interaction problem: towards Physics based stabilization techniques

J.C. Cajas* , C. Treviño** , G. Houzeaux* and M. Vázquez*
Corresponding author: juan.cajas@bsc.es

* Barcelona Supercomputing Center (BSC), Barcelona, Spain.
** UMDI, Facultad de Ciencias, Universidad Nacional Autónoma de México, Sisal, Yucatán, Mexico.

Abstract: Fluid-Structure Interactions is a very active research field and its potential and reach is out of question. In order to develop algorithms and coupling strategies to be employed in the modelling of Fluid Structure Interaction problems in a partitioned scheme, it is of special interest to gain insight in the regions where instabilities and other non-linear effects occur. The present contribution analyzes a well suited FSI case, complex enough to present all the physical relevant properties of the unstable region of interest, but simple enough to allow the use of linear stability analysis to identify and characterize the general unstable mechanisms common to FSI cases. The model will be introduced and results on the solid body trajectories, the synchronization mechanisms and the numerical stability of a loosely coupling algorithm will be presented. Similitudes with the canonical system of vortex induced vibrations of a two-degrees of freedom circular cylinder will be pointed out, suggesting interesting lines of future research.

Keywords: Numerical Algorithms, Computational Fluid Dynamics, Fluid-Structure interaction, Numerical stability.

1 Introduction

Fluid-Structure Interactions (FSI) govern so many physical problems, industrial devices, and biological systems that its relevance is evident. Two very complete overviews of the state of the art in FSI problems can be found in [1], [2], and references therein. A very common strategy to solve FSI problems is the partitioned or staggered approach, where the fluid and solid problems are solved in separated domains, and the solution of the full problem is achieved by the correct use of the physical coupling conditions. Numerous studies have focused in the development of this approach and have pointed out the most defiant problems of the formulation, for example [3, 4, 5]. In the previous contributions, besides the general theoretical framework for FSI, a very important difficulty is pointed out: the presence of the added mass effect, which is an instability arising for incompressible fluid flow and that depends on the fluid and solid densities, and can lead to unstable staggered schemes [6] [7]. Usually, the instability issues arising from FSI problems in the staggered approach have been treated numerically, with the use of relaxation factors or acceleration schemes [8].

In order to develop algorithms and coupling strategies to be employed in the modelling of Fluid Structure Interaction problems in a partitioned scheme, it is of special interest to gain insight in the regions where instabilities and other non-linear effects occur. The present contribution analyzes a well suited FSI case, complex enough to present all the physical relevant properties of the unstable region of interest, but simple enough to allow the use of linear stability analysis to identify and characterize the general unstable mechanisms common to FSI cases. With a deeper physical understanding, the development of coupling algorithms and physics-based stabilization techniques will be at hand. The proposed system is depicted in Fig.1 and is inspired in previous numerical simulations to study a new design of wind energy generator.

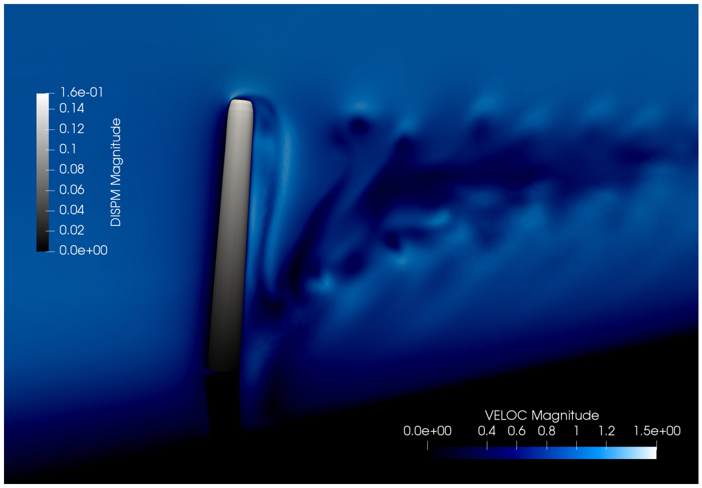

Figure 1: Typical instantaneous displacement and velocity fields for the studied system.

2 Problem Statement

The system under study is shown in Fig.1. It consists of a rigid mast of large aspect ratio $AR = 11$ fixed in its base with a torsion spring. The mast is embedded in a Newtonian viscous flow with constant velocity far upstream of the mast. The fluid is considered to be incompressible and to have constant viscosity. The problem is modelled as follows.

2.1 Fluid component

In the present contribution, the fluid part of the FSI problem will be modelled as an incompresible Newtonian fluid. The Navier-Stokes equations written in the Arbitrary Lagrangian Eulerian (ALE) formulation are employed. In this case the fluid conservation laws are written in a moving Eulerian domain and the governing equations are written in this frame of reference. This formulation is widely used [9, 10, 8, 11] therefore the steps to obtain the governing equations are not repeated herein. The resulting equations for a Newtonian viscous fluid are

$$\rho_f \frac{\partial \boldsymbol{u}_f}{\partial t} + \rho_f [(\boldsymbol{u}_f - \boldsymbol{u}_m) \cdot \nabla] \boldsymbol{u}_f - \mu_f \nabla^2 \boldsymbol{u}_f + \nabla p = \rho_f \boldsymbol{f}, \tag{1}$$

$$\nabla \cdot \boldsymbol{u}_f = 0. \tag{2}$$

Where $\boldsymbol{u}_f$ is the fluid velocity field, ρ_f is the fluid density, μ_f is the fluid viscosity, p is the pressure, $\boldsymbol{u}_m$ represents the domain velocity and $\boldsymbol{f}$ is the body force. In our implementation $\boldsymbol{u}_m$ is obtained from the domain displacement, $\boldsymbol{d}_m$, computed as the solution of a diffusion equation of the form

$$\nabla \cdot [c_m \nabla \boldsymbol{d}_m] = 0,$$

where c_m is a diffusion coefficient. At the discrete level, $\boldsymbol{d}_m$ is the node displacement and c_m is computed element-wise in order to control the stiffness of the elements. In our implementation, c_m is a discontinuous function computed as

$$c_m = AR/V,$$

with AR the aspect ratio and V the volume of the element. In this way, small elements and elements with large aspect ratio will be 'stiffer', which in practice is found to be useful in order to preserve the boundary layer elements.

2.2 Solid component

For the solid component of the coupled problem, the motion of the mast can be described as a top that is not allowed to spin over its symmetry axis and is only allowed to deviate from the vertical axis in two directions following a Hookean law in the angular displacements. A very convenient reference system to describe this motion is the one shown in Fig. 2, where an inertial system of reference is shown in lower case letters and a moving reference frame attached to the rigid body is shown in upper case letters.

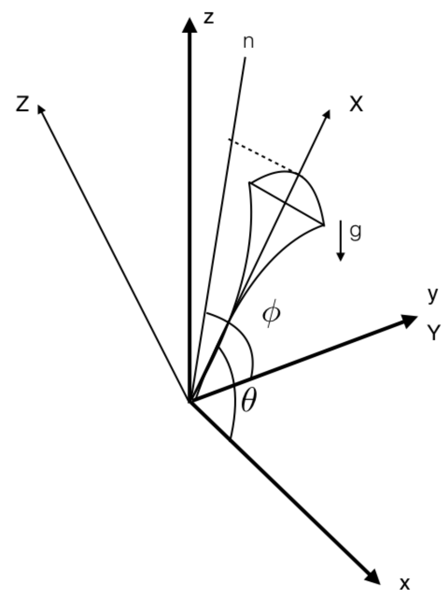

Figure 2: Vortex bladeless reference systems. Lowercase letters correspond to the inertial reference system and uppercase letters to the moving reference frame.

The Lagrangian function of such system can be obtained in a similar way as the one of the classical symmetric top resulting

$$L = T - V = \frac{1}{2}\left[I\left(\dot{\theta}^2 + \dot{\phi}^2 \sin^2\theta\right)\right] - mgh\sin\theta\sin\phi - \frac{kh^2}{2}((\theta-\pi/2)^2 + (\phi-\pi/2)^2), \tag{3}$$

where T is the kinetic and V the potential energy of the system, θ is measured from the x axis and ϕ is the angle between the projection of the symmetry axis of the rigid body to the yz plane and the y axis. I is the inertia tensor and h is the distance between the center of mass of the body and the fixed point, k is the spring stiffness and g the gravity acceleration. The resulting equations of motion are:

$$\begin{aligned} I\ddot{\theta} - I\dot{\phi}^2\sin\theta\cos\theta + mgh\cos\theta\sin\phi + kh^2(\theta-\pi/2) &= 0, \\ I\sin^2\theta\,\ddot{\phi} + mgh\sin\theta\cos\phi + kh^2(\phi-\pi/2) &= 0. \end{aligned} \tag{4}$$

Equations (4) are valid for the cases where the only external forces are gravity and the resistance in the fixed point of the body. In the case of the FSI problem, there will be a force coming from the interaction with the fluid that can not be written as the derivative of a known potential, we will call this force $\mathbf{F} = (F_x, F_y, F_z)$ and will assume its components are known in the inertial system of reference. In this case, the equations of motion will be derived from the general expression:

$$\frac{d}{dt}\left(\frac{\partial T}{\partial \dot{q}^j}\right) - \frac{\partial T}{\partial q^j} = Q_j, \tag{5}$$

where Q_j are the generalized forces. In our case, we can separate the generalized forces in those that can be written as the derivatives of a potential and those that can not in the form

$$Q_j = -\frac{\partial V}{\partial q^j} + Q_j^*.$$

With this separation, it is clear that the equations of motion will take the form

$$\begin{aligned} I\ddot{\theta} - I\dot{\phi}^2 \sin\theta\cos\theta + mgh\cos\theta\sin\phi + kh^2(\theta - \pi/2) &= Q_\theta^*, \\ I\sin^2\theta\,\ddot{\phi} + mgh\sin\theta\cos\phi + kh^2(\phi - \pi/2) &= Q_\phi^*. \end{aligned} \tag{6}$$

In eq.(6) Q_θ^* and Q_ϕ^* are generalized forces that can not be calculated simply by applying a transformation of coordinates to F_x, F_y, F_z because they are components of a vector and depend on the reference system in which they are written. In order to calculate them, the virtual work done in virtual displacements $\delta\theta$ and $\delta\phi$ will be calculated. First a virtual displacement $\delta\theta$ will be performed keeping ϕ fixed.

$$\delta w = (F_z\cos\theta - F_x\sin\theta)h\delta\theta$$

The generalized forces are the coefficients that multiply the virtual displacements in order to get the virtual work so:

$$Q_\theta^* = (F_z\cos\theta - F_x\sin\theta)\,h \tag{7}$$

If we perform a virtual displacement in the ϕ direction keeping θ fixed we obtain

$$Q_\phi^* = (F_z\cos\phi - F_y\sin\phi)\,h \tag{8}$$

And the equations of motion are then:

$$\begin{aligned} I\ddot{\theta} - I\dot{\phi}^2 \sin\theta\cos\theta + mgh\cos\theta\sin\phi + kh^2(\theta - \pi/2) - (F_z\cos\theta - F_x\sin\theta)\,h &= 0, \\ I\sin^2\theta\,\ddot{\phi} + mgh\sin\theta\cos\phi + kh^2(\phi - \pi/2) - (F_z\cos\phi - F_y\sin\phi)\,h &= 0. \end{aligned} \tag{9}$$

2.3 Dissipative forces

The dissipative forces in the fixed point are considered to vary linearly with the angular velocity in the form

$$D_\theta = -\alpha_\theta h\dot{\theta},$$

$$D_\phi = -\alpha_\phi h\dot{\phi},$$

with α_j as dissipation constants. The equations of motion are finally written as

$$\begin{aligned} I\ddot{\theta} - I\dot{\phi}^2 \sin\theta\cos\theta + mgh\cos\theta\sin\phi + kh^2(\theta - \pi/2) - (F_z\cos\theta - F_x\sin\theta)\,h + \alpha_\theta h^2\dot{\theta} &= 0, \\ I\sin^2\theta\,\ddot{\phi} + mgh\sin\theta\cos\phi + kh^2(\phi - \pi/2) - (F_z\cos\phi - F_y\sin\phi)\,h + \alpha_\phi h^2\dot{\phi} &= 0. \end{aligned} \tag{10}$$

2.4 Non-dimensional equations

Selecting the maximum diameter of the mast d as unit length and the magnitude of the inflow velocity u_0 as characteristic velocity we can define the non-dimensional variables $t^* = u_0\,t/d$, $x^* = x/d$, $\boldsymbol{u}^* = \boldsymbol{u}/u_0$. Using this set of variables the eqs. (1), (2) and the system (10) can be written as follow:

$$\frac{\partial \boldsymbol{u}_f^*}{\partial t} + [(\boldsymbol{u}_f^* - \boldsymbol{u}_m^*)\cdot\nabla]\boldsymbol{u}_f^* - \frac{1}{Re}\nabla^2\boldsymbol{u}_f^* + \nabla p^* = \boldsymbol{f}^*, \tag{11}$$

$$\nabla\cdot\boldsymbol{u}_f^* = 0, \tag{12}$$

with $Re = \rho_f u_o d/\mu_f$ the Reynolds number based on the maximum diameter of the mast.

$$\ddot\theta - \dot\phi^2\sin\theta\cos\theta + \frac{mgd^2h}{u_0^2\,I}\cos\theta\sin\phi + \frac{kd^2h^2}{u_0^2\,I}(\theta-\pi/2) - \frac{d^2\,h}{u_0^2\,I}(F_z\cos\theta - F_x\sin\theta) + \frac{dh^2\alpha_\theta}{u_0\,I}\dot\theta = 0,$$

$$\sin^2\theta\,\ddot\phi + \frac{mgd^2h}{u_o^2\,I}\sin\theta\cos\phi + \frac{k\,d^2h^2}{u_0^2\,I}(\phi-\pi/2) - \frac{d^2\,h}{u_o^2\,I}(F_z\cos\phi - F_y\sin\phi) + \frac{dh^2\alpha_\phi}{u_0\,I}\dot\phi = 0.$$

It is important to notice that the aerodynamic forces F_x, F_y and F_z will be result of the interaction of the mast with the fluid and will be of the form

$$F_i = \frac{1}{2}\rho_f\,u_o^2 C_i A$$

where A is a reference surface, approximated by $A = dl$ in our case, with $l > h$ the lenght of the mast. Then, it is possible to write the external force term in (13) as

$$\frac{2}{\pi m_r^*}(C_z\cos\theta - C_x\sin\theta),$$

with the reduced mass coefficient defined as

$$m_r^* = \frac{I/dh}{\pi(d/2)^2 l\rho_f},$$

which compares the mass of fluid displaced by the mast with its moment of inertia, and acts as an effective mass of the system. In a similar way, we can define the non-dimensional parameter:

$$m_{gr}^* = \frac{u_o^2 I}{mgd^2h},$$

that compares the influence of the gravity potential energy of the mast with the kinetic energy provided by the flow. Also, it is possible to define the reduced velocity

$$u_r^* = \frac{2\pi u_o}{\sqrt{k/(I/h^2)}d},$$

which is the natural frequency of the system scaled by the factor u_0/d. And for the dissipative forces the following non-dimensional parameter is defined

$$\zeta_i^* = \frac{\alpha_i}{2\sqrt{kI/h^2}}$$

With all the previous in mind the system (10) is written in non-dimensional form as

$$\ddot\theta - \dot\phi^2\sin\theta\cos\theta + \frac{1}{m_{gr}^*}\cos\theta\sin\phi + \left(\frac{2\pi}{u_r^*}\right)^2(\theta-\pi/2) - \frac{2}{\pi m_r^*}(C_z\cos\theta - C_x\sin\theta) + \left(\frac{4\pi}{u_r^*}\right)\zeta_\theta^*\dot\theta = 0,$$

$$\sin^2\theta\,\ddot\phi + \frac{1}{m_{gr}^*}\sin\theta\cos\phi + \left(\frac{2\pi}{u_r^*}\right)^2(\phi-\pi/2) - \frac{2}{\pi m_r^*}(C_z\cos\phi - C_y\sin\phi) + \left(\frac{4\pi}{u_r^*}\right)\zeta_\phi^*\dot\phi = 0. \tag{13}$$

This system of equations is very similar to the canonical case of the vortex induced vibrations (VIV) of a circular cylinder with two degrees of freedom studied in [12, 13, 14, 15] and references therein.

2.5 FSI coupling

In this contribution, it is of particular interest to explore the numerical unstable regions of the present mechanical system. Thus, no stabilizing techniques will be used and a loosely coupled algorithm will be employed. In one time step, the fluid mechanics problem is solved, the drag and lift are calculated and used to solve the rigid body equations, with the new location of the rigid body the fluid mesh is moved and the time step is advanced.

3 Numerical formulation

The following discretization schemes for the fluid and the rigid body mechanics problems were used: The Navier-Stokes equations were discretized using the stabilized finite element method, with Variational MultiScale stabilization, which is considered an implicit Large Eddy Simulation method, as explained in [16]. The unknowns of the problem are separated into grid scale components and subgrid scale components with the possibility of tracking the subgrid components in time and space to give more accuracy and stability to the numerical model. The momentum equation is separated from the continuity equation using the Schur complement for the pressure, each equation is solved independently and the solution of the coupled system is obtained in an iterative way. The time integration scheme used is a Backward Differentiation Formula of second order using a time step which guaranteed a CFL number lower than 10. The details and validation of the solution strategy are provided in [17, 18]. The rigid body equations were integrated in time using a fourth order Runge-Kutta method. A similar set-up adequate for turbulent FSI cases was used in [15] where validation an comparison with numerical and experimental results can be found.

The computational domain of the fluid represents a wind tunnel of 22 length units in the cross-flow direction and 220 length units in the in-flow direction, the mast is located at 55 length units of the wind tunnel entrance, where a unitary constant inflow velocity is imposed. The outflow is a free surface, the bottom wall and the mast are considered non-slip surfaces while the side and top walls of the wind tunnel are considered slip surfaces. The computational domain is discretized with 2.6 million elements, most of them tetrahedra. The simulation was run using 144 cores of the MareNostrum IV super computer.

4 Results

4.1 Numerical results

A fixed value of the Reynolds number with $Re = 100$ is selected with four combinations of the reduced velocity and mass. Also, without loss of generality, the influence of gravity is neglected and attention is focused in the balance between the aerodynamic forces and the restitutive forces of the spring. In future work, a more extensive study of the parameter space will be carried out. The parameters used at present are summarized in Table 1.

Case	m_r^*	u_r^*	ζ_θ^*, ζ_ϕ^*
1	5.49	6.05	0.015
2	3.29	4.69	0.022
3	2.63	4.19	0.025
4	2.19	3.83	0.027

Table 1: Parameters explored in the present work with a fixed value of the $Re = 100$ and negligible influence of gravity.

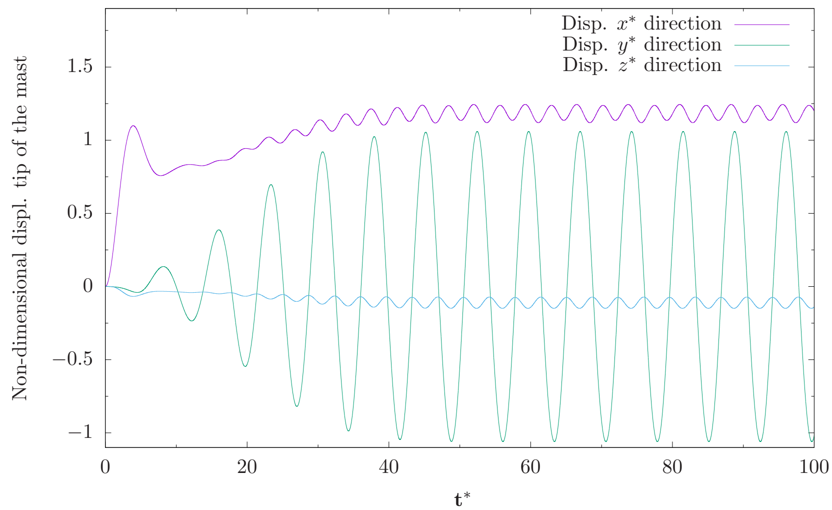

Figure 3: Temporal evolution of the displacement of the tip of the mast for case 1. The synchronization between the aerodynamic forces and the solid displacement provokes a rapid increase in the amplitude of the oscillation response of the body.

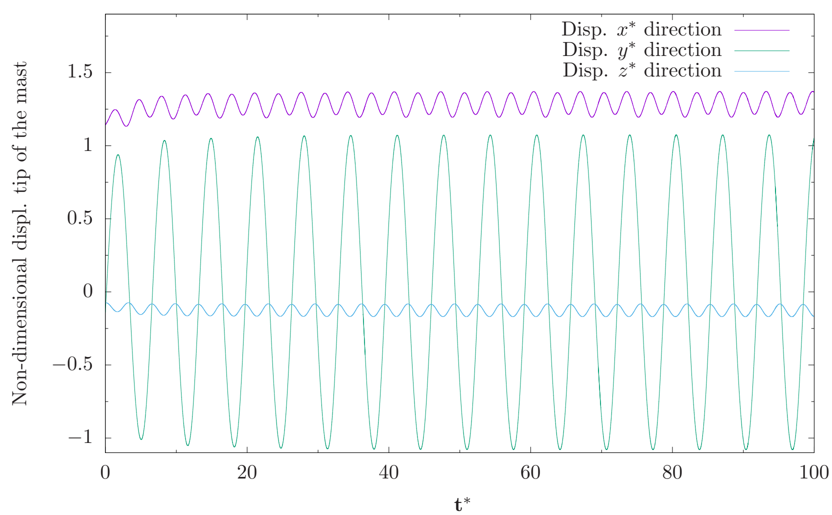

Figure 4: Temporal evolution of the displacement of the tip of the mast for case 2. After a short transient synchronized state is reached and regular oscillations are obtained.

An initial developed velocity field with $Re = \rho_f u_o d/\mu_f = 100$ with the mast fixed was chosen as initial condition for case 1, then the FSI simulation was started and evolved until a final periodic state was reached. Then this state was used as initial condition for case 2, the final oscillatory state of case 2 was used as initial condition of case 3 and similarly the final oscillatory state of case 3 is used as the initial state for case 4. The temporal evolution of the displacement of the tip of the mast for the studied cases for the first 100 time units in the x, y and z directions are shown in Figs.3-6, where small variations in the final total amplitude of the displacement is observed but clear differences in the frequency of the oscillatory response are obtained. This shows that the system is able to synchronize at different frequencies in a very similar way as the two-degrees of freedom circular cylinder does, see for example the results in [13]. It is noted that the loosely coupling algorithm is not robust enough for case 4, where a quick crash is obtained in the simulation.

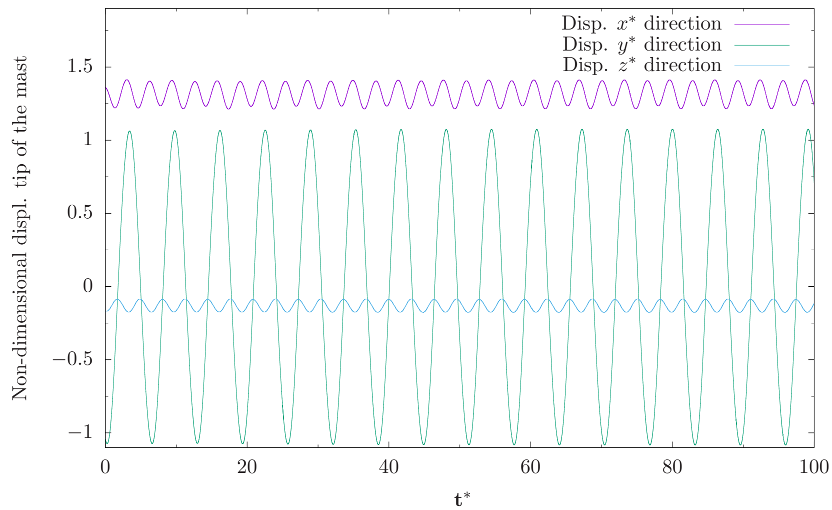

Figure 5: Temporal evolution of the displacement of the tip of the mast for case 3. As in case 2, a short transient followed by a regular oscillatory state is reached quickly.

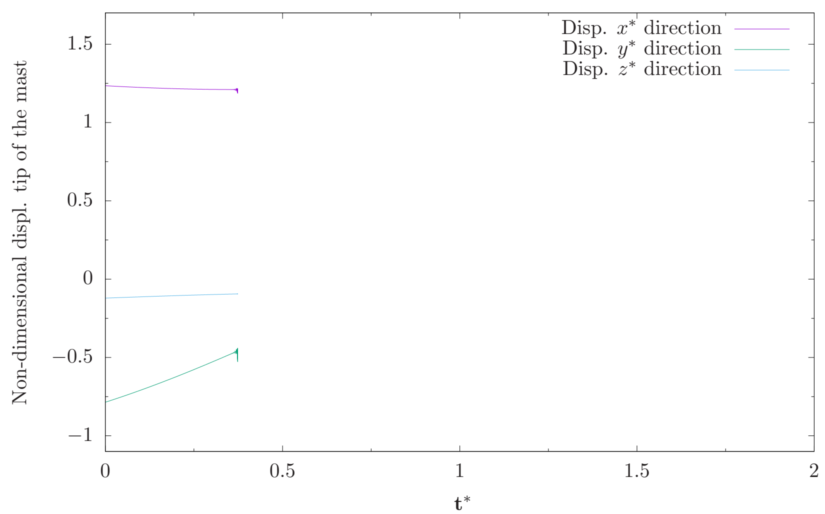

Figure 6: Temporal evolution of the displacement of the tip of the mast for case 4. The loosely coupled algorithm is not robust enough and a quick crash in the simulation is obtained.

The synchronization mechanism of this system is illustrated in Fig. 7, where the lift coefficient and the y direction displacement of the tip of the mast for case 2 are plotted. The equivalent graphs for the other cases show similar trends. It is pointed out that there is a shift in the phases of both curves. The dark area shows the time lapses when the lift force favours the displacement of the mast, while the clear area shows the lapses where the lift force opposes the movement of the body. The differences in the length of the lapses provides the necessary work to induce the vibrations.

The trajectories described by the tip of the mast, as well as their projections to the xy and the xz planes are shown in Figs.8-11 for all the studied cases. It is pointed out that the projections to the xy plane of the trajectories of cases 1-3 are remarkably similar to those found in the two-degrees of freedom circular cylinder case, for example see the results in [15]. However, an extra degree of freedom is present in the studied system and the resulting trajectories are 3D. The extra degree of freedom links the effect of the areodynamic forces,

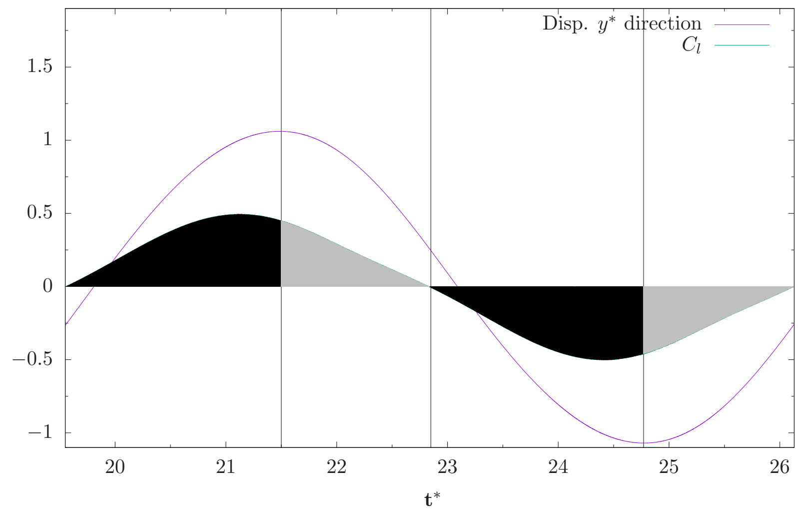

Figure 7: Synchronization mechanism in case 2. The dark area shows the time lapses when the lift force favours the displacement of the mast. The clear area shows the lapses where the lift force opposes the movement of the body.

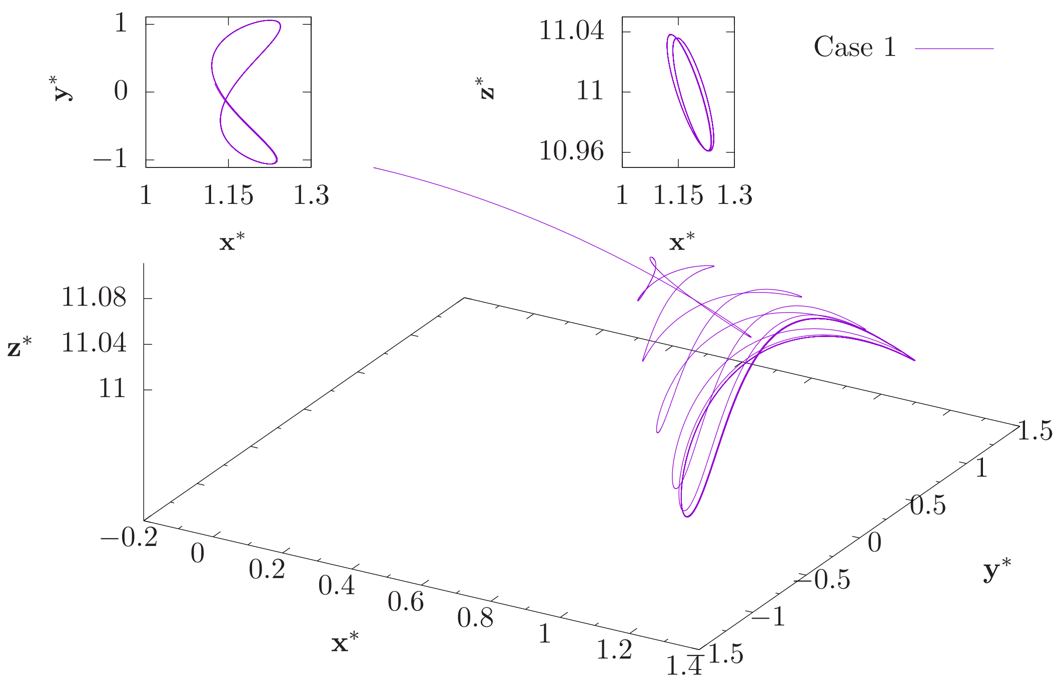

Figure 8: Trajectory of the tip of the mast for case 1. An initial deviation from the starting position in the in-flow direction followed by the amplification of the oscillations in the cross-flow direction are observed. The final closed trajectory is shown in the xy and xz projections.

as can be seen from eq. (13). This suggests that important differences with the two-degrees of freedom circular cylinder may be found and further research in this direction is needed. Also, considering all the mentioned similarities, it is of great interest to explore if a three branches response as the one described in

[12, 14, 15] is present in this system as well.

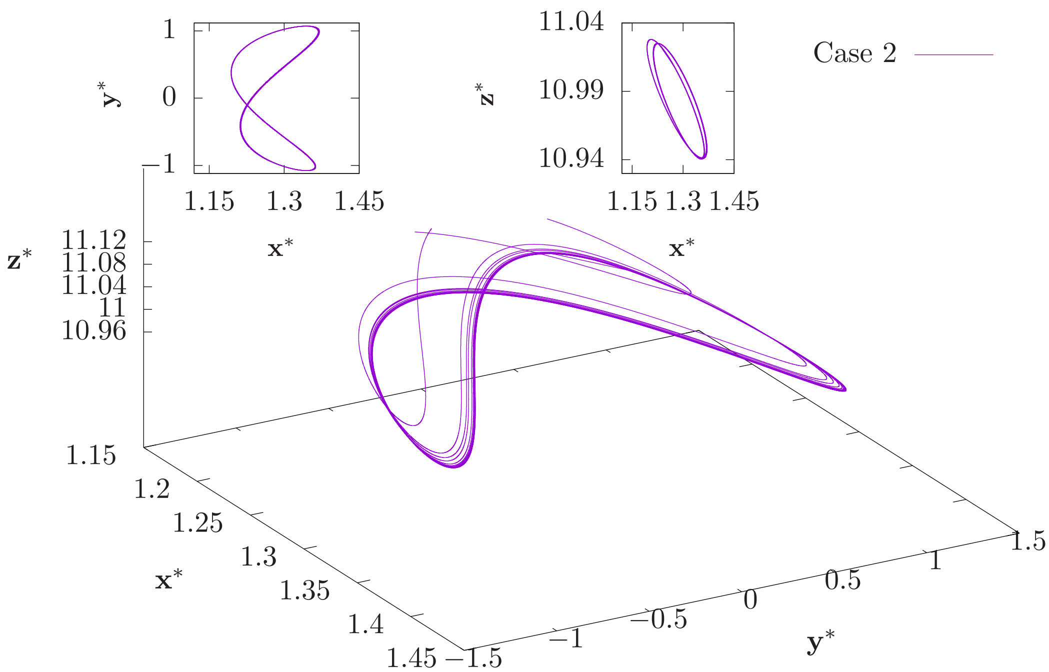

Figure 9: Trajectory of the tip of the mast for case 2. After a short transient state, a final closed trajectory is reached and shown in the xy and xz projections.

On the other hand, case 4 shows a high frequency oscillatory deviation from the expected trajectory and a final crash on the simulation is obtained. It is very interesting that the deviation of the expected trajectory observed in Fig. 11 occurs in such a way that suggests that the displacement of the mast creates a pressure gradient in the fluid that opposes its movement. This pressure gradient results to be large enough to displace the mast in the opposite direction, creating an even larger pressure gradient which opposes the movement again and so on. In the authors' opinion, this is the same instability as the well known added mass effect in FSI problems. This configuration results in a numerical instability triggered by physical means, so the authors propose to investigate this numerical instability from a physical perspective.

4.2 Stability properties of the solutions

The stability analysis of the system will be carried out in a similar way as done in [19], and the numerical instability of the loosely coupled algorithm will be investigated from a physical perspective. The linear stability problem will be posed using eqs. (11), (12) and (13) and the solutions obtained in Sec. 4.1 will be used as the base FSI configuration. Numerical eigenfunctions will be constructed and the stability problem will be solved.

This is an on-going work, but some results are already available. In order to construct the numerical eigenfunctions, a rapidly decaying perturbation will be applied to the base flow. The perturbation will be a high frequency external force applied to the mast with the following form

$$F_{pi} = F_i \left(1 + \varepsilon\, e^{-t^*/\tau^*} \sin(\omega_p t^*)\right)$$

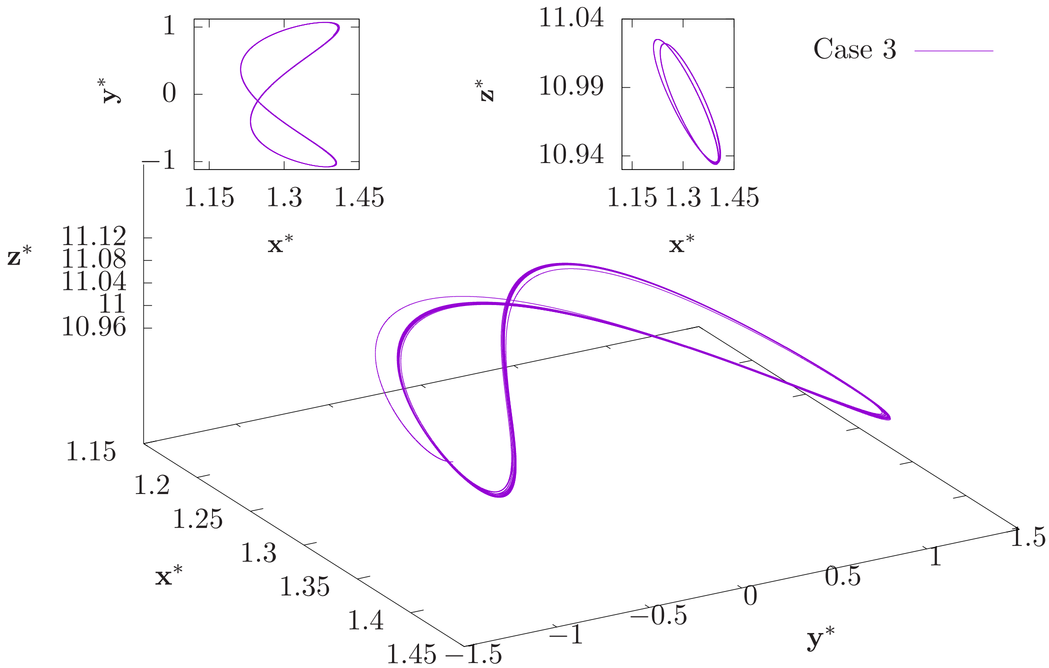

Figure 10: Trajectory of the tip of the mast for case 3. After a short transient state, a final closed trajectory is reached and shown in the xy and xz projections.

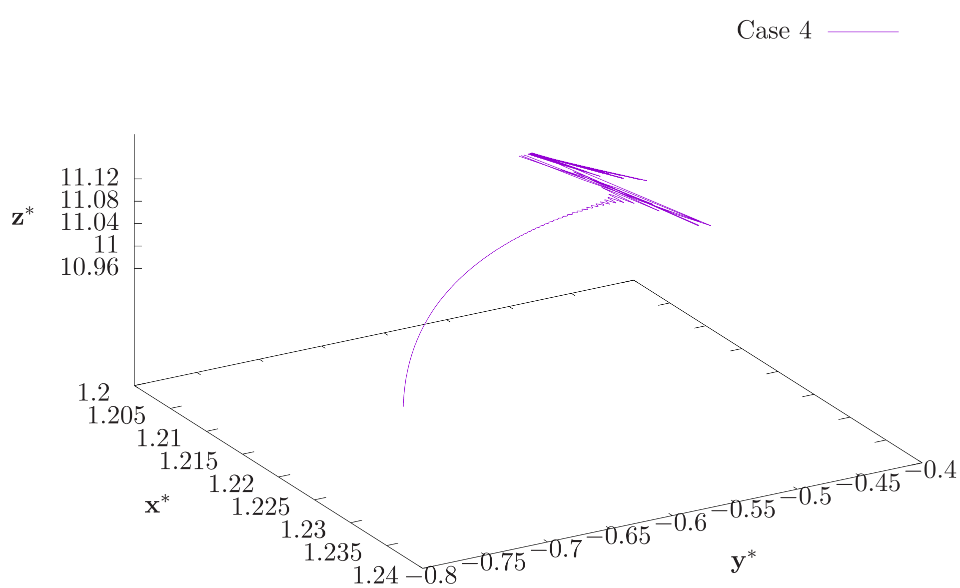

Figure 11: Trajectory of the tip of the mast for case 4. A high frequency oscillatory deviation from the expected trajectory and a final crash on the simulation is obtained

where ε is a non-dimensional parameter very small compared with unity, τ^* is a non-dimensional parameter to control the perturbation's amplitude decay and ω_p is its non-dimensional frequency. In the present work a value of $\omega_p = 17$ is selected, which means that the perturbation will have a frequency ~ 20 times larger than the C_l coefficient of case 1. Then the system will be allowed to evolve in time for a lapse of 5τ and the last cycle solution will be saved. The normalized difference between this solution and the base flow will be the numerically generated eigenfunction and will be the initial condition of the linear stability analysis.

5 Conclusion and Future Work

A three dimensional FSI model was introduced and mathematically described. The governing equations were solved numerically and results on the solid body trajectories, the synchronization mechanisms and the numerical stability of a loosely coupling algorithm were presented. Similitudes with the canonical system of VIV of a two-degrees of freedom circular cylinder where exposed and interesting lines of research are proposed. In the authors' opinion, the numerical instabilities encountered are triggered by physical means and a physics based linear stability analysis is proposed as future work. Some results available in this direction were also presented.

References

[1] Yuri Bazilevs, Kenji Takizawa, and Tayfun E. Tezduyar. *Front Matter, in Computational Fluid-Structure Interaction: Methods and Applications*. John Wiley & Sons, Ltd, Chichester, UK, 2013.

[2] Thomas Richter. *Fluid-structure Interactions*, volume 118 of *Lecture Notes in Computational Science and Engineering*. Springer International Publishing, 2017.

[3] Tayfun E. Tezduyar, Sunil Sathe, Ryan Keedy, and Keith Stein. Space-time finite element techniques for computation of fluid-structure interactions. *Computer Methods in applied mechanics and engineering*, 195:2002–2027, 2006.

[4] Wolfgang A. Wall, Steffen Genkinger, and Ekkehard Ramm. A strong coupling partitioned approach for fluid-structure intraction with free surfaces. *Computers & fluids*, 36(1):169–183, 2007.

[5] S. Wang, B.C. Khoo, G. R. Liu, and G. X. Xu. An arbitrary lagrangian-eulerian gradient smoothing method (gsm/ale) for interaction of fluid and a moving rigid body. *Computers & fluids*, 71(30):327–347, 2013.

[6] Christiane Förster, Wolfgang A. Wall, and Ekkehard Ramm. Artificial added mass instabilities in sequential staggered coupling of nonlinear structures and incompressible viscous flow. *Computer methods in applied mechanics and engineering*, 196(7):1278–1293, 2007.

[7] P. Causin, J.F. Gerbeau, and F. Nobile. Added-mass effect in the design of partitioned algorithms for fluid-structure problems. *Computer Methods in applied mechanics and engineering*, 194:4506–4527, 2005.

[8] W. Dettmer and D. Perić. A computational framework for fluid-structure interaction: Finite element formulation and applications. *Computer methods in applied mechanics and engineering*, 195:5754–5779, 2006.

[9] Charbel Farhat, Michel Lesoinne, and Patrick LeTallec. Load and motion transfer algorithms for fluid/structure interaction problems with non-matching discrete interfaces: Momentum and energy conservation, optimal discretization and application to aeroelasticity. *Computer methods in applied mechanics and engineering*, 157:95–114, 1998.

[10] Ulrich Küttler and Wolfgang A. Wall. Fixed-point fluid-structure interaction solvers with dynamic relaxation. *Computational mechanics*, 43(1):61–72, 2008.

[11] Tayfun E. Tezduyar. Finite elements in fluids: Stabilized formulations and moving boundaries and interfaces. *Computers & fluids*, 36(2):191–206, 2007.

[12] N. Jauvtis and C. H. K. Williamson. The effect of two degrees of freedom on vortex-induced vibration at low mass and damping. *Journal of Fluid Mechanics*, 509:23–62, 2004.

[13] J M Dahl, F S Hover, M S Triantafyllou, S Dong, and G. E. Karniadakis. Resonant vibrations of bluff bodies cause multivortex shedding and high frequency forces. *Physical Review Letters*, 99(14):5–8, 2007.

[14] Simon Gsell, Rémi Bourguet, and Marianna Braza. Two-degree-of-freedom vortex-induced vibrations of a circular cylinder at Re=3900. *Journal of Fluids and Structures*, 67:156–172, 2016.

[15] D Pastrana, JC Cajas, O Lehmkuhl, I Rodríguez, and G Houzeaux. Large-eddy simulations of the vortex-induced vibration of a low mass ratio two-degree-of-freedom circular cylinder at subcritical reynolds numbers. *Computers & Fluids*, 2018.

[16] O. Colomés, S. Badia, R. Codina, and J. Principe. Assessment of variational multiscale models for the large eddy simulation of turbulent incompressible flows. *Computational methods in applied mechanics and engineering*, 285:32–63, 2015.

[17] G. Houzeaux and J. Principe. A variational subgrid scale model for transient incompressible flows. *Int. J. CFD*, 22(3):135–152, 2008.

[18] G. Houzeaux, R. Aubry, and M. Vázquez. Extension of fractional step techniques for incompressible flows: The preconditioned orthomin(1) for the pressure schur complement. *Computers & Fluids*, 44(1):297–313, 2011.

[19] Lorenzo Martínez-Suástegui, César Treviño, and J. C. Cajas. Steady and oscillatory laminar opposing mixed convection in a vertical channel of finite length subjected to symmetrical isothermal discrete heat sources. *Physics of Fluids*, 27(6):063604, 2015.